Research Article | Vol. 28, No. 24 / 23 November 2020 / Optics Express 35528
Optics EXPRESS

Design of two invisibility cloaks using transmissive and reflective metamaterial-based multilayer frame microstructures

XUFENG JING,[1,2] DANTIAN FENG,[1] YING TIAN,[1] MENG LI,[1,2] CHENGFEI CHU,[1,2] CHENXIA LI,[1] YINGWEI HE,[3,4] HAIYONG GAN,[3,5] AND ZHI HONG[2]

[1]*Institute of Optoelectronic Technology, China Jiliang University, Hangzhou 310018, China*
[2]*Centre for THz Research, China Jiliang University, Hangzhou 310018, China*
[3]*National Institute of Metrology, Beijing, China*
[4]*heyw@nim.ac.cn*
[5]*ganhaiyong@nim.ac.cn*

Abstract: Ultrathin metamaterials provide new possibilities for the realization of cloaking devices because of their ability to control electromagnetic waves. However, applications of metamaterials in cloaking devices have been limited primarily to reflection-type carpet cloaks. Hence, a transmissive free-space cloak was developed using a multilayer frame structure, wherein highly transparent metamaterials were used to guide incident waves into propagating around an object. The cloaking effect was quantitatively verified using near-field and far-field distributions. Metamaterials allow for the cloaking shells of transmissive cloaks to be developed without spatially varying extreme parameters. Moreover, a transmissive invisible cloak with metamaterial-based mirrors was designed. The design principle of this cloak with a frame structure consists of four metamaterial-based mirrors and two metal mirrors. After covered with the designed metamaterials-based mirrors cloak, the outgoing electromagnetic wave is restored greatly as if the wave passes directly through the obstacle without distortion. This cloak used the metamaterials mirrors to adjust the reflected angle, so that the outgoing electromagnetic wave does not change direction, thereby achieving the cloaking effect.

1. Introduction

The realization of invisibility has always been a significant goal and has inspired considerable research. The concept of the invisibility cloak has attracted significant attention from the scientific community in the past decade [1]. Metamaterials provide routes to manipulating electromagnetic (EM) waves [2–7] as a method for achieving cloaking and invisibility [8–16]. Early cloaks were designed mainly based on transformation optics (TO) [17], with which EM waves can be guided around a hidden object via control over the complex distribution of spatial permittivity and permeability. Such cloaks indeed cause the target object to appear invisible. However, this method generally requires bulk metamaterials to satisfy the requirements for some anisotropic and inhomogeneous material parameters. Based on this background, some simplified methods, such as quasi-conformal mapping [18] and homogeneous coordinate transformation [19], have been proposed. However, the resulting cloaks are bulky and suffer from loss, which makes them difficult to use in a laboratory. To overcome bulkiness, plasmonic cloaks based on scattering cancellation have been developed [20]. These devices can produce cloaking effects while having small thicknesses, but usually perform poorly under high-sensitivity detection. Other methods, such as the use of near-zero refractive index metamaterials [21] and microstrip patch antennas [22], which can also direct EM wave energy around hidden objects, have also been used to create cloaking devices.

#409137 https://doi.org/10.1364/OE.409137
Journal © 2020 Received 2 Sep 2020; revised 28 Oct 2020; accepted 28 Oct 2020; published 9 Nov 2020

Optics EXPRESS

Recently, metamaterials, which are artificially ultrathin layers, have attracted significant attention from researchers. These materials have extraordinary control over the phases, amplitudes, and polarizations of incident waves. Metamaterials can break the thickness limits of conventional cloaks that have been developed based on metamaterials [23]. As a result, metamaterials provide possibilities for the design of an effective invisibility cloak. Several metamaterial-based carpet cloaks that can control the phases of reflected waves to restore the near-field wavefront have been proposed. Metamaterial-based carpet cloaks have many advantages, such as low loss, high shapeability, ease of fabrication, and high flexibility. However, metamaterial-based carpet cloaks based on local phase compensation operate predominantly in the reflection mode. Although several designs for transmissive metamaterial-based cloaks have already been explored [24–27], the transmissive cloak developed in this study may substantially widen the practical applicability of metamaterial-based cloaks.

In this paper, the design of a transmissive invisibility cloak based on a multilayer frame structure of metamaterials is proposed. Such a metamaterial cloak increases the capability of traditional cloaks to achieve the transmissive mode. The developed cloak can considerably simplify the design and experimental process of TO-based cloaks, which currently require complex material parameters and a complex spatial distribution. The proposed invisibility cloak is composed of three metamaterials, the functions of which are beam splitting, steering, and collection of incident waves. With this cloak, the near-field wavefront of the transmitted EM wave can be effectively restored, and scattering can be minimized. Numerical simulations not only verify the cloaking effect but also create possibilities for the design of a transmissive cloak while avoiding the use of complex material parameters.

2. Cloaking theory

Currently, metamaterials are widely used in ultrathin carpet cloaks because of their extraordinary control over the phases and amplitudes of waves. Such metamaterials are composed of many unit cells, which permit local phase compensation to be accomplished through variations in the size parameters of the unit cells. In this study, a transmissive metamaterial-based cloak was developed based on a novel three-layer frame structure composed of metamaterials. Figure 1(a) shows a schematic diagram of the new invisibility cloak based on this metamaterial frame structure, where a *y*-polarization plane wave with normal incidence through the invisibility cloak can bypass the obstacle and emerge as a plane wave.

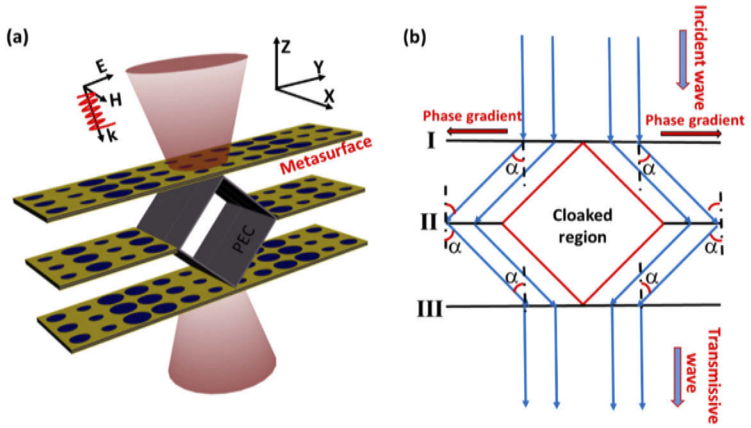

Fig. 1. (a) 3D scheme of transmissive invisibility cloak. (b) Schematic diagram of transmissive metamaterial cloak. I, II, III represent three transparent metamaterials with their respective phase gradients.

Optics EXPRESS

To control the refraction, the generalized Snell's law of refraction is used [23]:

$$\sin\theta_t - \sin\theta_i = \frac{\lambda_0}{2\pi}\frac{d\varphi}{dx}, \tag{1}$$

where θ_i and θ_t are the incident angle and angle of refraction, respectively; λ_0 is the working wavelength; and $d\varphi/dx$ is the phase gradient. From Eq. (1), the refraction angle can be entirely controlled through variations in the transmitted phase gradient. Based on this idea, a transmissive invisibility cloak based on metamaterials can be realized. The principle of the metamaterial-based transmissive cloak is demonstrated as follows. Figure 1(b) shows the design principle of this cloak, specifically a multilayer frame structure, which consists of three metamaterials, referred to herein as I, II, and III. A plane wave with *y*-polarization is normally incident on metamaterial I. The left and right sides of the three metamaterials have opposite phase gradients. Therefore, for the left side of metamaterial I, the relationship between the angle of refraction and the phase gradient can be expressed as

$$\sin(-\alpha) - \sin(\theta_0) = -\frac{\lambda_0}{2\pi}\frac{d\varphi_1}{dx}. \tag{2}$$

Meanwhile, for the right side of metamaterial I, this relationship can be expressed as

$$\sin(\alpha) - \sin(\theta_0) = \frac{\lambda_0}{2\pi}\frac{d\varphi_1}{dx}. \tag{3}$$

Similarly, the left and right sides of the metamaterials II and III can be denoted as

$$\sin(\alpha) - \sin(-\alpha) = -\frac{\lambda_0}{2\pi}\frac{d\varphi_2}{dx}, \tag{4}$$

$$\sin(-\alpha) - \sin(\alpha) = \frac{\lambda_0}{2\pi}\frac{d\varphi_2}{dx}, \tag{5}$$

$$\sin(\theta_0) - \sin(\alpha) = -\frac{\lambda_0}{2\pi}\frac{d\varphi_3}{dx}, \tag{6}$$

$$\sin(\theta_0) - \sin(-\alpha) = \frac{\lambda_0}{2\pi}\frac{d\varphi_3}{dx}, \tag{7}$$

where α is the value of each corresponding angle, and $\theta_0 = 0^\circ$ when a plane wave is normally incident on the metamaterials. Moreover, $d\varphi_1/dx$, $d\varphi_2/dx$, and $d\varphi_3/dx$ are the phase gradients of metamaterials I, II, and III, respectively. Based on the principles expressed in Eqs. (1)–(7), a plane wave can eventually bypass obstacles via beam splitting, steering, and collection performed by the metamaterials, thus restoring the wavefront and achieving a cloaking effect.

3. Transmissive metamaterial-based cloak

To develop the metamaterials for creating the cloak, we designed a coaxial circular hole structure, shown in Fig. 2(a). Each metamaterial is composed of an array of coaxial annular apertures. The unit cell of the metamaterial is composed of a three-layer coaxial metal structure with a circular hole and two layers of a dark-blue dielectric structure. Copper was chosen as the metal material to be used on the metamaterials. The loss due to metallic materials cannot be eliminated by designing different structures, and this is an intrinsic loss. All dielectric unit structures with relatively larger refractive index (n>2) can be applied to construct a transmission-type stealth device. Metasurfaces utilize dielectric materials with (n>2) to cover the phase range of 0–2π can be used to remove the intrinsic loss of metallic materials. Each metal layer, which had a thickness of 0.04 mm, was perforated with a round hole. Each dielectric layer had a thickness of 1.6 mm and a relative dielectric permittivity of $\varepsilon = 2.65$. The selected dielectric material with $\varepsilon = 2.65$ for transmissive cloak in the manuscript is F4B dielectric material. This dielectric material exists in nature, and this permittivity value is realistic. The period of the unit cell was $p = 12$ mm. The radius of the hole is denoted as *inr*, which had a variable value. Through variations in the

Optics EXPRESS

radius of the hole, a phase change from 0 to 2π could be accomplished. Figure 2(b) shows the amplitudes and phases of different unit cells under normal incidence and at an oblique incidence of 38.7°. In Fig. 2(b), the dashed line indicates the amplitude of the transmitted wave, whereas the solid line signifies the phase change as a function of the radius of the hole. The transmitted wave could perform a phase change at 2π, and the amplitude could reach values higher than 0.75, which ensured that most of the transmitted energy could be preserved. In Fig. 2(c), (a) plane wave is normally incident on metamaterial I (left part), and the EM is bent to a refraction angle of $\alpha = 38.7°$ at 10 GHz. For metamaterial I, the phase gradient is 90°, and a refraction angle of $\alpha = 38.7°$ can be obtained. Figure 2(d) depicts the far-field radiation pattern of the transmitted wave for metamaterial I, which is consistent with the theoretical value of the deflection angle. The key components on this design are the three layers of gradient metasurface lens, which has been intensively investigated in recent years. In general studies of flat lens, their main function is focusing. In our paper, we stack the three layers of lenses together to achieve the restoration of the beam front and achieve the stealth effect through three processes of electromagnetic beam splitting, polarization and convergence. In our paper, three flat lens are skillfully applied to the design of transmission stealth device, which extends the application range of flat lens.

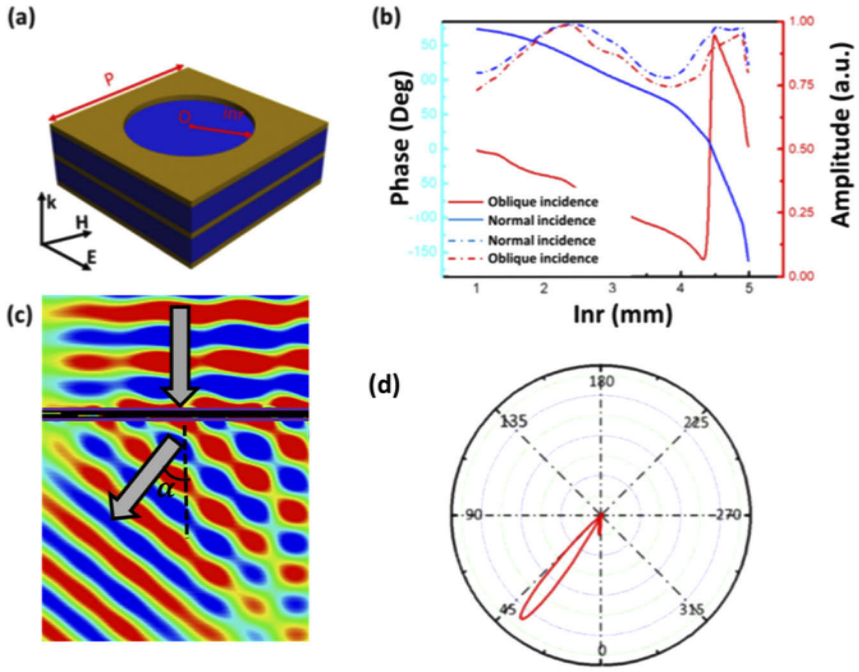

Fig. 2. (a) Unit cell of proposed metamaterials. Each unit cell consists of three-layer coaxial metal and two-layer dielectric substrate with permittivity of 2.65. Periods along x and y directions are $P = 12$ mm; thickness of metal is 0.04 mm, and thickness of substrate is 1.6 mm; radius *inr* is variable. (b) Amplitude and phase of transmitted waves with respect to change in *inr*. (c) Electric field distribution when y-polarization plane wave is incident on metamaterial I (left part). (d) Far-field radiation pattern for transmitted wave bent by metamaterial I at 10 GHz.

Based on the characteristics of the metamaterials and the design principle illustrated in Fig. 1, (a) transmissive invisibility cloak can be designed with a three-layer frame structure, as shown in Fig. 1(a). The region to be cloaked was restricted by a metallic diamond with a side length of 153.5 mm. The height along the z-axis was 240 mm. Because of the limitations in terms of the simulation conditions, the left and right sides along the y-axis were set at $24\lambda_0$, where λ_0 is the

Optics EXPRESS

working wavelength at 10 GHz in free space. The cloak was assumed to be infinitely long in the x direction. To validate the design, a full-wave simulation was performed using the finite integral method. Open boundaries were applied in the y and z directions, whereas the boundary condition in the x direction was set to be periodic.

To verify the cloaking effect, the effectiveness of the designed cloak was quantitatively checked via comparisons between the near-field distributions for an obstacle without and with the cloak, as shown in Fig. 3. The electric field distribution of a diamond-shaped obstacle, shown in Fig. 3(a), indicates strong distortion in the transmitted wavefront at 10 GHz. Meanwhile, two side lobes are due to the edge reflection of the metallic diamond. After the object was covered with the designed metamaterial cloak, as shown in Fig. 3(b), the field intensity was distributed as if there was no obstacle. The wavefront of the electric field for the frame structure of the designed cloak underwent beam splitting, steering, and collection, and finally emerged without the distortion. For practical applications, cloaking devices cannot be infinite in the x- direction. Eight unit structures were arranged in x-direction with the open boundary condition, and the electric field distribution with cloaking shell is shown in Fig. 3(c). It can be seen that the electric field distribution is slightly changed compared with that in Fig. 3(b). The small change in electric field intensity is due to the finite size in the x direction. Stealth effect is also obvious.

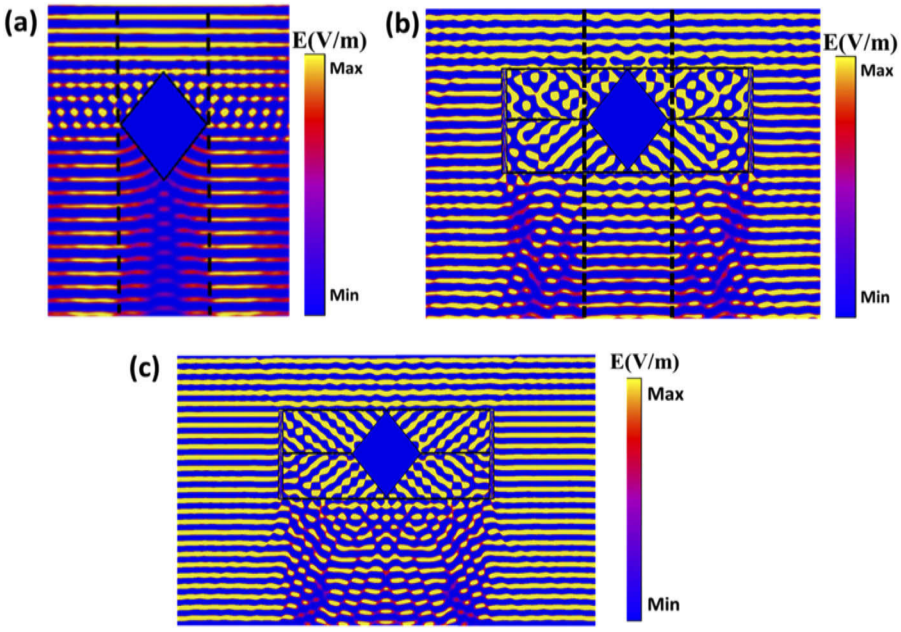

Fig. 3. (a) Electric field distribution for bare diamond obstacle. (b) Electric field distribution with cloaking shell. (c) Electric field distribution for the cloaking with eight unit structures at x-direction.

Figures 4(a) and 4(b) present the local electric field distributions within the black dotted area marked in Fig. 3 for the bare diamond-shaped obstacle and the cloaking device, respectively. Figures 4(c) and 4(d) show the power flow distributions for the diamond obstacle without and with the metamaterial cloak, respectively, at 10 GHz. It can be clearly seen that the metamaterial-based cloak produces a favorable cloaking effect. The forward scattering wavefront of the obstacle can be reconstructed by the designed cloak, as shown in Fig. 4(b).

For the bare obstacle, a strong scattering is observed, with almost no energy arising on the back of the obstacle, as shown in Fig. 4(c). Correspondingly, for the cloaked obstacle, the incident EM energy impinging on the metamaterial cloak can bypass the obstacle and flow to the rear of

Optics EXPRESS

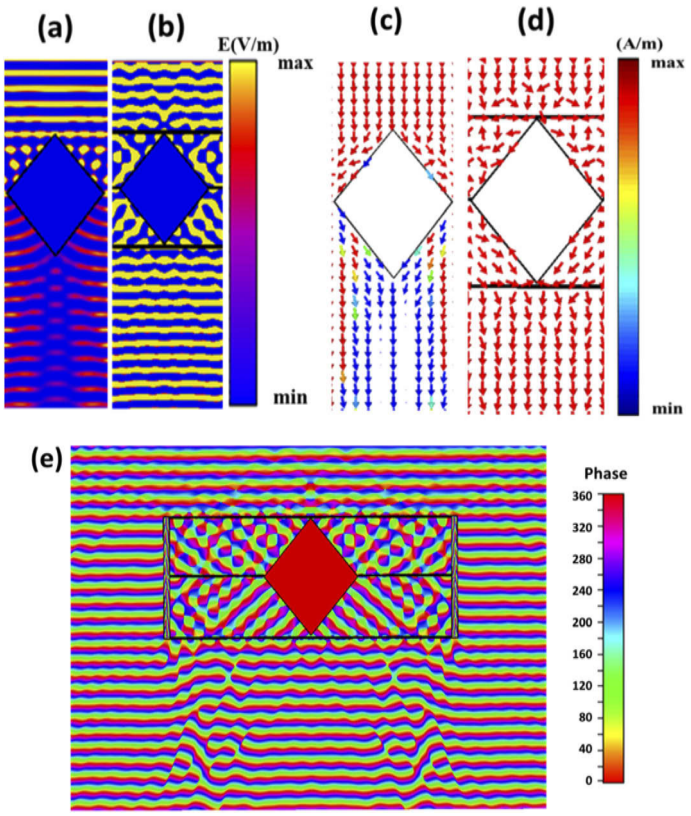

Fig. 4. (a) Local electric field distribution for bare diamond obstacle (denoted in Fig. 3(a) with black dotted line). (b) Local electric field distribution for cloaking shell (denoted in Fig. 3(b) with black dotted line). (c) Power flow without cloak. (d) Power flow with cloak. (e) The corresponding wavefront phase distribution.

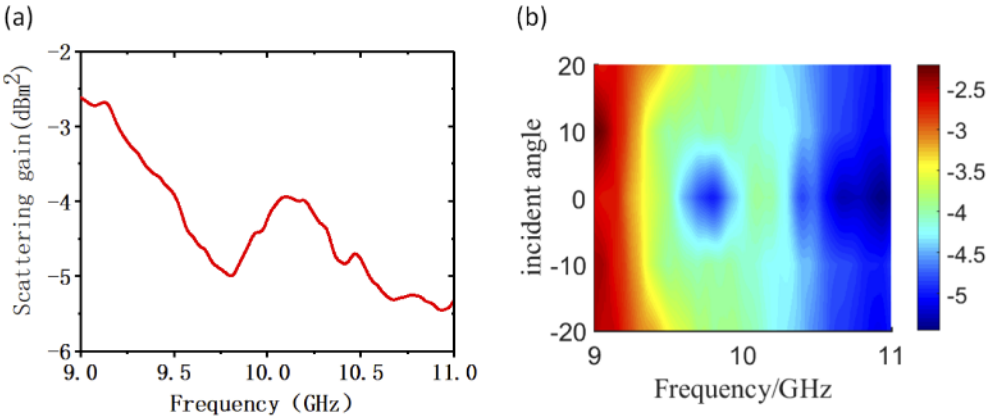

Fig. 5. Total scattering gain of invisibility cloak. (a) Scattering gain of invisibility cloak as function of frequency at normal incidence. (b) Two-dimensional color map of scattering gain under different incident angles.

Optics EXPRESS

the obstacle, as though the barrier does not exist, as visualized in Fig. 4(d). The corresponding wavefront phase distribution is shown in Fig. 4(e).These characteristics confirm the cloaking effect produced by the proposed device. In addition, the cloak designed in this research is feasible for experimental preparation [24–37]. It should be noted that E.Bor *et al.* proposed the design of a directional optical cloaking by a genetic algorithm, and this cloaking can be realized experimentally [38]. The optimization algorithm designs the permittivity distribution of the dielectric polylactide material to achieve an optical cloaking effect [38]. Although our designed cloaking device and the reported cloaking device used different methods, both the designed cloaks had obvious effect.

To quantitatively evaluate the invisibility performance of this transmissive cloak, the total scattering gain was calculated as a function of frequency at normal incidence, as shown in Fig. 5(a). The total scattering gain of cloaks is defined in detail in Ref. [28]. The radar cross

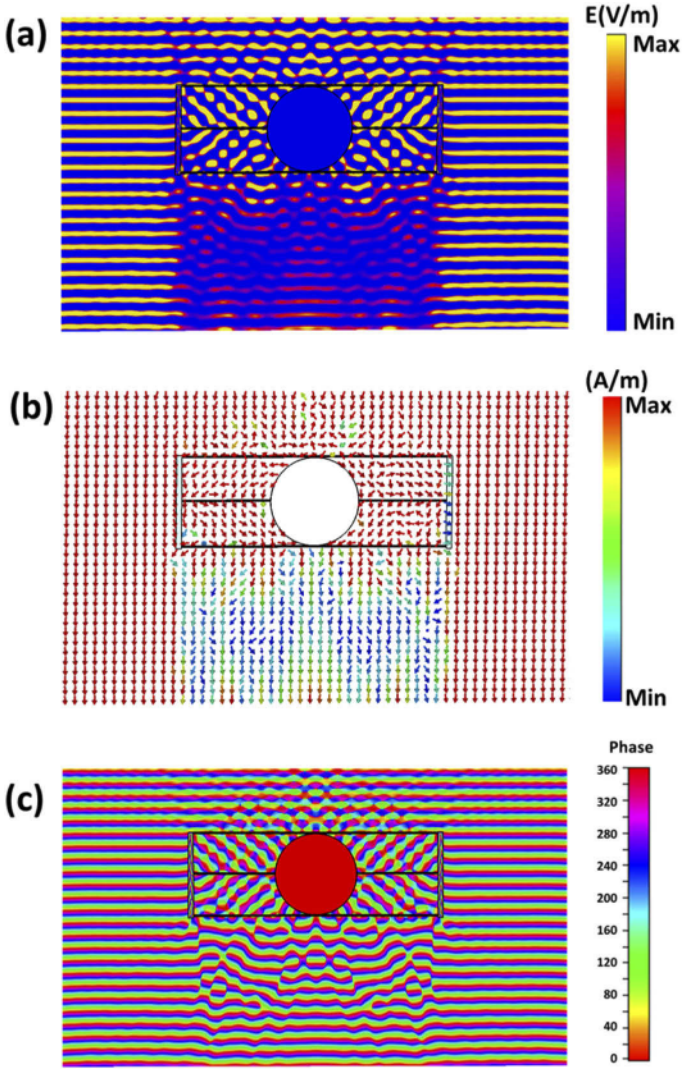

Fig. 6. (a) Electric field distribution for the cylindrical obstacle with cloaking. (b) Power flow with cloak. (c) The corresponding wavefront phase distribution.

Optics EXPRESS

section (RCS) of the cloaked obstacle was suppressed by approximately 4.5 dB at 10 GHz at normal incidence. As shown in Fig. 5(b), the cloak exhibits RCS suppression over a relatively large bandwidth and angular span. As shown in Fig. 5(b), it seems that the designed cloak around 11 GHz has better performance with suppressing more scattering at wider angles of incidence than at 10 GHz. But, we originally designed metamaterials to construct cloaking device at 10 GHz. This may be attributed to the difference of simulated boundary conditions between the designed metamaterial unit cell and the whole cloaking device. In order to construct a metamaterial stealth device, we first need to optimize the design of metamaterial unit structure. During the optimization design of the unit structure, the periodic boundary condition in numerical simulations was used to calculate the phase change at 10 GHz. However, when we calculated the metamaterial cloaking device, the open boundary condition was used to calculate the stealthy device characteristics. So, the larger suppression frequency is shifted to about 11 GHz.

In the case of rectangular (diamond-shaped) cloak, the travelling wave inside the cloak propagates in parallel with the surface of the rectangular cloak. As a result, scatterings do not occur since the light does not hit the object surface. In order to further reflect the practical application, the diamond-shaped PEC can be replaced by a cylindrical scatterer object. The radius of the circle is equal to the distance between the metamaterial layers. Figure 6(a) shows the electric field distribution for the cylindrical obstacle with the metamaterials-based cloaking. The transmitted near-field wavefront was restored considerably, which created an illusion of the wave passing directly through the obstacle without distortion. Because the circular structure has strong scattering against the incident wave, the amplitude of the electric field intensity tends to decrease when the incident wave passes through the cloaking device. Figure 6(b) shows the power flow distribution for the cylindrical obstacle with the metamaterial cloak. The corresponding wavefront phase distribution is shown in Fig. 6(c). It can be clearly seen that the metamaterial-based cloak produces a favorable cloaking effect.

4. Metamaterial mirror-based cloaking

A transmissive invisibility cloak with metamaterial-based mirrors, as shown in Fig. 7, was also designed in this study. A schematic diagram of the designed cloak is shown in Fig. 7(a). Four metamaterial mirrors were used to control the reflective EM wave, and two metal mirrors on both sides of the rhombus frame were used to reflect waves from the metamaterial-based mirrors. Figure 7(b) shows the design principle of this cloak with a frame structure that consists of four metamaterial-based mirrors, labeled I, II, III, and IV, and two metal mirrors. If all mirrors are metallic, the degree of freedom of design will be severely limited. The ordinary metal reflector strictly obeys Snell's law for incident light and reflected light, and the incident angle is equal to the reflected angle. Therefore, replacing a metamaterial mirror with a metal mirror requires a strict design and a fixed cloaked region. However, for the metamaterials reflectors, they can realize the free regulation of the reflected light's reflection angle based on the gradual distribution of reflected phase. The incidence angle can be different from the reflection angle, and the stealth area can be changed with the change of the adjustment angle. Therefore, metamaterials reflectors have a greater degree of freedom than ordinary metal reflectors. To ensure better control over the propagation direction of reflected waves from the metamaterial mirrors, the generalized Snell's law of reflection from Eqs. (1)–(7) was used to design the mirrors. The reflective angle of the metamaterials can entirely be controlled using variations in the phase gradient. The incident angle and the reflective angle were set as $\theta_1 = 45^\circ$ and $\beta = 78.18^\circ$, respectively.

To produce the metamaterial mirrors, a unit structure for building the mirrors, as shown in Fig. 8(a), was designed. Each unit cell was composed of a two-layer square metal structure and a layer of polyimide dielectric. The metal material was copper, and the dielectric material used had a relative permittivity of $\varepsilon = 3.5$. The thicknesses of the upper and lower layers of the metal were both $d1 = 0.2$ μm, and the polyimide thickness was $d2 = 30$ μm. The period of the unit cell was

Optics EXPRESS

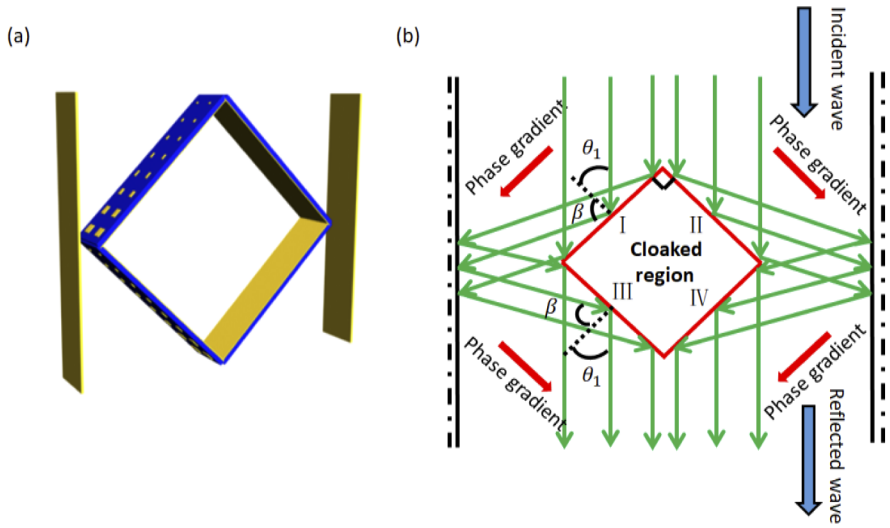

Fig. 7. (a) 3D scheme of transmissive invisibility cloak with metamaterial-based mirrors. (b) Schematic diagram of principle of cloaking.

p = 138 μm. The length a and width b of the metal layer in the unit cells were variable, and the different reflection phases were obtained mainly through changes in a and b; thereby, the gradient metamaterials that were required in this study were constructed. A bottom metal layer was used to enhance reflection. The specific structural parameters of the unit structures used to construct the metamaterials are shown in detail in Fig. 8(c). In Fig. 8(b), (a) plane wave is incident on metamaterial I (left part), and the EM wave is bent at a reflective angle of $\beta = 78.18°$ at 1 THz.

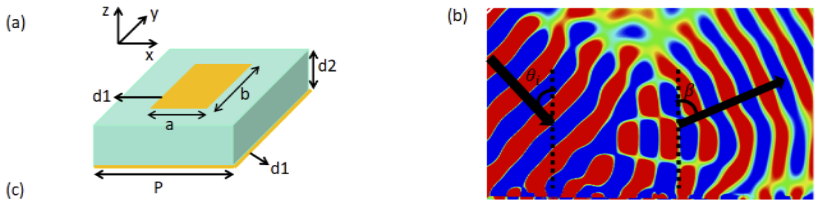

(c)

Structure shape / Parameter								
Variable (a)	a=100	a=60	a=40	a=90	a=50	a=110	a=50	a=40
Variable (b)	b=107	b=80	b=70	b=60.2	b=60	b=49.9	b=49.5	b=20
Phase	0	45	90	135	180	225	270	315
Reflection amplitude	0.9344	0.9905	0.9713	0.9721	0.9613	0.9743	0.9835	0.9951

Fig. 8. (a) Unit cell of proposed metamaterial-based mirrors. Each unit cell consists of sandwich structure with two copper layers of 0.2 μm thickness separated by 30 μm thick polyimide and with permittivity of 3.5. Periods along x and y directions are both p = 138 μm. (b) Electric field distribution when y-polarization plane wave is incident on metamaterial mirror I. (c) Specific parameters of metamaterial structure.

To verify the cloaking effect, the effectiveness of the designed cloak was quantitatively evaluated based on comparisons between the distributions of electric field and power flow between the bare

Optics EXPRESS

and cloaked obstacles, as shown in Fig. 9. The presented reflective device requires two mirrors to operate as a cloak. As can be seen from Fig. 9, the simulation region is bounded by two mirrors in one direction. According to Fig. 7, the minimum distance between mirrors and cloaked object can be calculated. According to $\theta = 33.18°$, $m = 1656$ μm, $y = m * \sin 45° = 1170.969$ μm, so $\tan\theta = \frac{y}{x+y}$. Then, the distance can be calculated as $x = 405.272$ μm. The utilization of presented reflection-based cloak is limited to certain scenarios due to the requirement two side mirrors. Figure 9(a) shows the electric field distribution of the bare diamond-shaped obstacle. At a 1-THz operating frequency, most of the energy of the EM wave was observed to be scattered by the obstacle. After the obstacle was covered with the designed metamaterial-based mirror cloak, as shown in Fig. 9(b), the outgoing EM wave was restored considerably, which made the wave appear as though it has passed directly through the obstacle without distortion. This structure uses mainly the metamaterial mirrors to adjust the reflected angle of the wave, such that the outgoing EM waves do not change direction; thereby a cloaking effect is achieved.

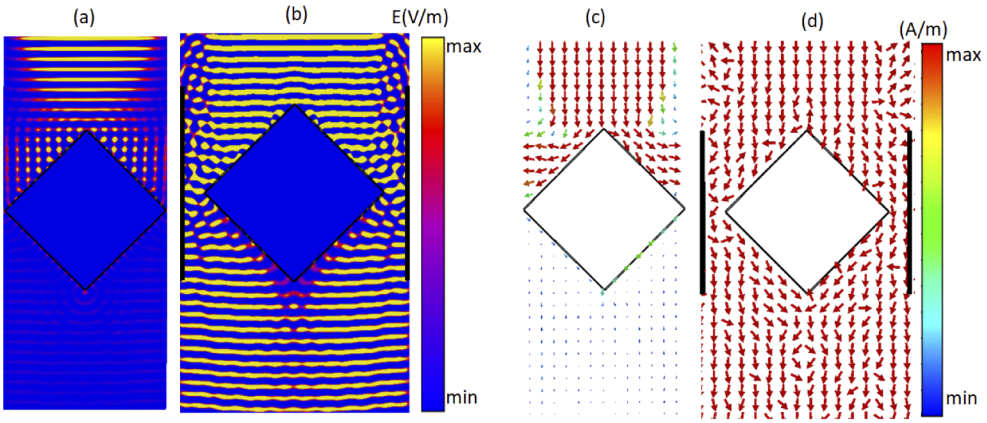

Fig. 9. (a) Electric field distribution for bare diamond obstacle. (b) Electric field distribution with cloaking structure. (c) Power flow without cloak. (d) Power flow with cloak.

Figures 9(c) and 9(d) show the power flow distributions for the bare diamond obstacle and cloaked obstacle, respectively. For the bare obstacle, a strong scattering is observed, with almost no energy arising on the back of the obstacle, as shown in Fig. 9(c). When covered by the cloak, the diamond obstacle is bypassed by the power flow, which results in substantial energy behind the obstacle, as shown in Fig. 9(d).

To quantitatively evaluate the invisibility performance of the mirror-based cloak, the total scattering gain of the cloak, shown in Fig. 10, was calculated. The RCS of the cloaked obstacle was suppressed by approximately 1.3 dB at 1 THz at normal incidence, as shown in Fig. 10(a). As shown in Fig. 10(b), the cloak exhibits RCS suppression over a relatively large bandwidth and angular span.

These two kinds of transmission stealth devices are mainly designed and applied in the case of vertical incidence. If the incidence angle is increased, the stealth effect will be significantly reduced. Although the total scattering cross section of the designed stealth devices can be reduced within a certain angle, the designed stealth device is not suitable for wide angle range. The cloaking devices we designed mainly used the free deflection characteristic of the electromagnetic beam by using metamaterials. In the case of the diamond-shaped cloak, the travelling wave inside the cloak propagates in parallel with the surface of the rectangular cloak. As a result, scatterings do not occur since the light does not hit the object surface. The electromagnetic beam can bypass the obstacle and realize wave front recovery. If cloaked region changes to sphere or ellipsoid, the scattering effect will occur, and the cloaking effect will be greatly reduced.

Optics EXPRESS

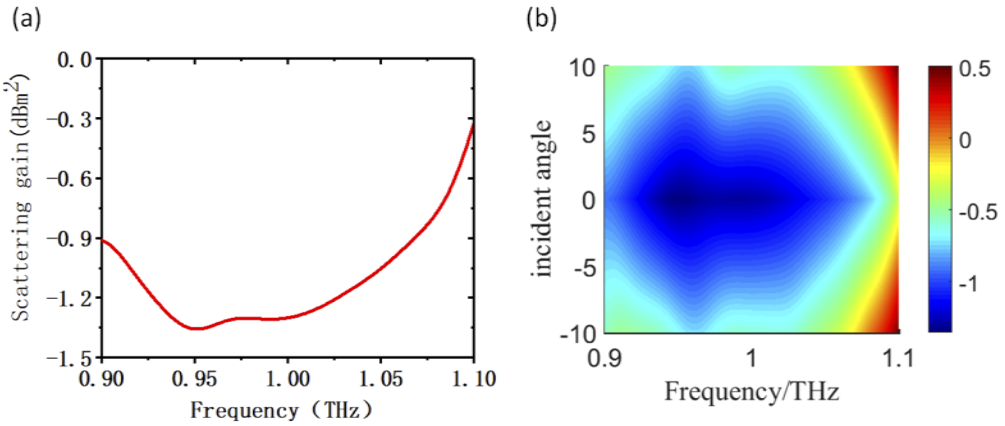

Fig. 10. (a) Total scattering gain of metamaterial-based mirrors invisibility cloak at normal incidence. (b) Two-dimensional color map of total scattering gain as function of angle of incidence and frequency.

5. Conclusions

A transmissive metamaterial cloak based on a frame structure composed of metamaterial layers was presented in this paper. The designed cloak is different from a TO-based cloak, which requires complex material parameters and spatial distribution. This cloak can guide EM waves into propagating around an object, thus creating an ideal hidden free space. The proposed cloak has a simple spatial structure, which simplifies its manufacturing for practical experiments. We also designed a transmitted invisible cloak with the metamaterials-based mirrors. Four metamaterials mirrors were used to control the reflective electromagnetic wave, and two metal mirrors on both sides of rhombus frame were also used to reflect the incoming wave from the metasurface-based mirrors. The application of the cloak can also be easily extended to other frequency domains, and the cloak can conceal large obstacles when carefully designed.

Funding

National Key Research and Development Program of China (2017YFF0206103); National Institute of Metrology Fundamental Research Project (No. AKYZD1909&2004); Natural Science Foundation of Zhejiang Province (LY20F050007, LZ21A040003); National Natural Science Foundation of China (61875179).

Disclosures

The authors declare no conflicts of interest.

References

1. D. Schurig, J. Mock, B. Justice, S. Cummer, J. Pendry, A. Starr, and D. Smith, "Metamaterial electromagnetic cloak at microwave frequencies," Science **314**(5801), 977–980 (2006).
2. X. He and H. Lu, "Graphene-supported tunable extraordinary transmission," Nanotechnology **25**(32), 325201 (2014).
3. X. He, "Tunable terahertz graphene metamaterials," Carbon **82**, 229–237 (2015).
4. H. Guan, H. Chen, J. Wu, Y. Jin, F. Kong, S. Liu, K. Yi, and J. Shao, "High-efficiency, broad-bandwidth metal/multilayer-dielectric gratings," Opt. Lett. **39**(1), 170–173 (2014).
5. X. He, X. Zhong, F. Lin, and W. Shi, "Investigation of graphene assisted tunable terahertz metamaterials absorber," Opt. Mater. Express **6**(2), 331–342 (2016).
6. M. Akram, G. Ding, K. Chen, Y. Feng, and W. Zhu, "Ultrathin Single Layer Metasurfaces with Ultra-Wideband Operation for Both Transmission and Reflection," Adv. Mater. **32**(12), 1907308 (2020).

Optics EXPRESS

7. M. Akram, M. Mehmood, X. Bai, R. Jin, M. Premaratne, and W. Zhu, "High Efficiency Ultrathin Transmissive Metasurfaces," Adv. Opt. Mater. **7**(11), 1801628 (2019).
8. K. Bi, D. Yang, J. Chen, Q. Wang, H. Wu, C. Lan, and Y. Yang, "Experimental demonstration of ultra-large-scale terahertz all-dielectric metamaterials," Photonics Res. **7**(4), 457–463 (2019).
9. Z. Bai, Q. Zhang, and G. Huang, "Nonlinear polaritons in metamaterials with plasmon-induced transparency," Chin. Opt. Lett. **17**(1), 012501 (2019).
10. N. Landy and D. Smith, "A full-parameter unidirectional metamaterial cloak for microwaves," Nat. Mater. **12**(1), 25–28 (2013).
11. D. Rusby, C. Armstrong, G. Scott, M. King, P. McKenna, and D. Neely, "Effect of rear surface fields on hot, refluxing and escaping electron populations via numerical simulations," High Power Laser Sci. Eng. **7**(3), e45 (2019).
12. X. Luo, Z. Tan, C. Wang, and J. Cao, "A reflecting-type highly efficient terahertz cross-polarization converter based on metamaterials," Chin. Opt. Lett. **17**(9), 093101 (2019).
13. R. Thomas, T. McManus, O. Teruel, S. Horsley, and Y. Hao, "Perfect surface wave cloaks," Phys. Rev. Lett. **111**(21), 213901 (2013).
14. K. Pan, D. Yang, L. Guo, Z. Li, S. Li, C. Zheng, S. Jiang, B. Zhang, and X. He, "Enhancement of the surface emission at the fundamental frequency and the transmitted high-order harmonics by pre-structured targets," High Power Laser Sci. Eng. **7**(2), e36 (2019).
15. I. Koirala, C. Park, S. Lee, and D. Choi, "Angle tolerant transmissive color filters exploiting metasurface incorporating hydrogenated amorphous silicon nanopillars," Chin. Opt. Lett. **17**(8), 082301 (2019).
16. A. Hanuka, K. Wootton, Z. Wu, K. Soong, I. Makasyuk, R. England, and L. Schächter, "Cumulative material damage from train of ultrafast infrared laser pulses," High Power Laser Sci. Eng. **7**(1), e7 (2019).
17. D. Shin, Y. Urzhumov, Y. Jung, G. Kang, S. Baek, M. Choi, H. Park, K. Kim, and D. Smith, "Broadband electromagnetic cloaking with smart metamaterials," Nat. Commun. **3**(1), 1213 (2012).
18. H. Ma and T. Cui, "Three-dimensional broadband ground-plane cloak made of metamaterials," Nat. Commun. **1**(1), 21 (2010).
19. H. Chen, B. Zheng, L. Shen, H. Wang, X. Zhang, N. Zheludev, and B. Zhang, "Ray-optics cloaking devices for large objects in incoherent natural light," Nat. Commun. **4**(1), 2652 (2013).
20. A. Alù, "Mantle cloak: invisibility induced by a surface," Phys. Rev. B **80**(24), 245115 (2009).
21. M. Silveirinha and N. Engheta, "Theory of supercoupling, squeezing wave energy, and field confinement in narrow channels and tight bends using ε near-zero metamaterials," Phys. Rev. B **76**(24), 245109 (2007).
22. J. Wang, S. Qu, Z. Xu, H. Ma, J. Zhang, Y. Li, and X. Wang, "Super-thin cloaks based on microwave networks," IEEE Trans. Antennas Propagat. **61**(2), 748–754 (2013).
23. N. Yu and F. Capasso, "Flat optics with designer metasurfaces," Nat. Mater. **13**(2), 139–150 (2014).
24. W. Zhao, H. Chu, Z. Tao, and Z. H. Hang, "Acoustic transmissive cloaking using zero-index materials and metasurfaces," Appl. Phys. Express **12**(5), 054004 (2019).
25. H. Chu, Q. Li, B. Liu, J. Luo, S. Sun, Z. H. Hang, L. Zhou, and Y. Lai, "A hybrid invisibility cloak based on integration of transparent metasurfaces and zero-index materials," Light: Sci. Appl. **7**(1), 50 (2018).
26. E. Shokati, N. Granpayeh, and M. Danaeifar, "Wideband and multi-frequency infrared cloaking of spherical objects by using the graphene-based metasurface," Appl. Opt. **56**(11), 3053–3058 (2017).
27. S. Liu, H. Xu, H. Zhang, and T. Cui, "Tunable ultrathin mantle cloak via varactor-diode-loaded metasurface," Opt. Express **22**(11), 13403–13417 (2014).
28. B. Orazbayev, N. Estakhri, A. Alù, and M. Beruete, "Experimental demonstration of metasurface-based ultrathin carpet cloaks for millimeter waves," Adv. Opt. Mater. **5**(1), 1600606 (2017).
29. S. Teng, Q. Zhang, H. Wang, L. Liu, and H. Lv, "Conversion between polarization states based on metasurface," Photonics Res. **7**(3), 246–250 (2019).
30. W. Zhu, M. Jiang, H. Guan, J. Yu, H. Lu, J. Zhang, and Z. Chen, "Tunable spin splitting of Laguerre–Gaussian beams in graphene metamaterials," Photonics Res. **5**(6), 684–688 (2017).
31. M. Jiang, H. Lin, L. Zhuo, W. Zhu, H. Guan, J. Yu, and Z. Chen, "Chirality induced asymmetric spin splitting of light beams reflected from an air-chiral interface," Opt. Express **26**(6), 6593–6601 (2018).
32. Y. Fu, Y. Fei, D. Dong, and Y. Liu, "Photonic spin Hall effect in PT symmetric metamaterials," Front. Phys. **14**(6), 62601 (2019).
33. C. Xi, P. Wang, X. Li, and Z. Liu, "Highly efficient continuous-wave mid-infrared generation based on intracavity difference frequency mixing," High Power Laser Sci. Eng. **7**(4), e67 (2019).
34. Y. Fu, Y. Xu, and H. Chen, "Negative refraction based on purely imaginary metamaterials," Front. Phys. **13**(4), 134206 (2018).
35. Z. He, Y. Zhu, and H. Wu, "Self-folding mechanics of graphene tearing and peeling from a substrate," Front. Phys. **13**(3), 138111 (2018).
36. S. Rubin and Y. Fainman, "Nonlinear, tunable, and active optical metasurface with liquid film," Adv. Photonics **1**(06), 1 (2019).
37. Z. Song, Q. Chu, X. Shen, and Q. Liu, "Wideband high-efficient linear polarization rotators," Front. Phys. **13**(5), 137803 (2018).
38. E. Bor, C. Babayigit, H. Kurt, K. Staliunas, and M. Turduev, "Directional invisibility by genetic optimization," Opt. Lett. **43**(23), 5781–5784 (2018).